Fabrication and Soft Magnetic Properties of $Fe_{81.3}Si_4B_{10}P_4Cu_{0.7}$ Amorphous Powders by Using the Spinning-water Atomization Process

Jiawei LI [1,2], Zihao XU [1], Zhenhua DAN [1,2]*, Hui CHANG [1], Akhiro MAKINO [3]

[1] *College of Materials Science and Engineering/ Tech Institute for Advanced Materials, Nanjing Tech University, No. 5 Xinmofan Road, Gulou District, Nanjing 210009, China*

[2] *Institute for Materials Research, Tohoku University, 2-1-1 Katahira, Aoba Ku, Sendai 980-8577, Japan*

[3] *Tohoku University, 2-1-1 Katahira, Aoba Ku, Sendai 9808577, Japan*

Soft magnetic $Fe_{81.3}Si_4B_{10}P_4Cu_{0.7}$ powders have been fabricated by using spinning-water atomization process (SWAP) under the water pressure of 17.5 MPa and gas pressure of 2 MPa. To clarify the amorphous forming ability, thermal stability, and the corresponding soft magnetism, the as-SWAPed powders have been sieved into 6 groups with different powder sizes of $0-150$ μm. After the analysis of the amorphous and crystalline characteristics, the morphology, and soft magnetic properties of these 6 groups of as-SWAPed powders, it is concluded that the SWAPs with a high cooling rate about 10^5 K/s can improve the amorphous forming abilities of $Fe_{81.3}Si_4B_{10}P_4Cu_{0.7}$ powders up to 53 μm, the saturated magnetic flux density as high as $170-173$ emu/g and the thermal stabilities higher than 112.8 K. The characteristic parameters of as-SWAPed powders above mentioned are close to those of the counterpart rapid solidified ribbons. The surface oxide layers on as-SWAPed powders mainly consist of Fe_3O_4 and SiO_2, and are 10 nm thick, much thicker than these counterpart ribbons, which might help to weaken the eddy effects accompanying with the slight decrease of the saturated magnetic flux density. Due to the higher cooling rates of SWAPs than gas atomization processes and the better spheroidization of powders for SWAPs than water atomization processes, it is key for NANOMET® family alloys to increase their amorphous forming abilities and better the soft magnetic performances.

Keywords: spinning-water atomization process, $Fe_{81.3}Si_4B_{10}P_4Cu_{0.7}$ amorphous powders, amorphous forming ability, thermal stability, soft magnetic performance.

1. INTRODUCTION

With the miniaturization of electronic products and the improvement of soft magnetic performance, the demand for high saturated magnetic density magnetic core materials is increasing. Registered iron-based soft magnetic materials, such as METGLAS ($Fe_{78}Si_9B_{13}$), NANOPERM (FeZr(Nb)BCu), FINEMET ($Fe_{73.5}Cu_1Nb_3Si_{13.5}B_9$), SENDUST ($Fe_{85}Si_{9.6}Al_{5.4}$) and other commercial alloys, cannot meet the current high saturated magnetic density requirements because of their lower iron content [1–4]. In recent years, NANOMET® soft magnetic alloys represented by $Fe_{83.3}Si_4B_8P_4Cu_{0.7}$ alloys have shown great potential for massive applications due to their good saturated magnetic induction densities, low core loss, and high permeabilities [5, 6]. NANOMET® soft magnetic alloy with saturated magnetic densities (B_m) higher than 1.5 T is mainly prepared by the rapid solidification method, that is the so-called single copper roll spinning method with a cooling rate as high as 10^6 K/s and flash annealing [7–9]. So far, the largest size of Fe-based amorphous soft magnetic alloy ($Fe_{66}Co_{15}Mo_1P_{7.5}C_{5.5}B_2Si_3$) have been reported being 2 mm, and its B_s is 1.65 T and $\Delta T(\Delta T = T_{x1}-T_{x2})$ is only 44 K [10]. Insufficient amorphous forming abilities of the Fe-based ribbons, usually less than 30 μm, limit their extensive applications [1, 5, 8]. Electric spark sintering (SPS) method [11] or additive manufacturing (3D printing, selective laser

remelting, hot isostatic pressing, etc.) [12–14] can effectively improve the final geometrical sizes, mechanical and magnetic properties of Fe-based amorphous soft magnets. Mahbooba et al. has succeeded to fabricate completely amorphous $Fe_{48}Cr_{15}Mo_{14}C_{15}B_6Er_2$ alloy with a critical thickness of 12 mm by a direct laser sintering [12]. The methods above require higher thermal stability, better spheroidization, and a larger amorphous forming ability for the raw powders. However, crystallization and rapid growth of crystals in Fe-based amorphous powders may cause a rapid coercivity increase. Therefore, it is urgent for raw powders to improve their thermal stability and forming ability.

Conventional methods including gas atomization, water atomization, mechanical ball milling, etc. have been used for preparing the metallic powders. The cooling rates of the gas atomization and water atomization are about 10^2 and 10^3 K/s [15–19]. Fully amorphous $Fe_{72}Si_{10.7}B_{10.7}Cr_{2.2}P_{1.5}C_{2.9}$ powders with good sphericity, smooth surface, uniform structure and high saturated magnetic flux density of 167.61 A·m²/kg have been successfully obtained through the water-gas combined atomization with a higher cooling rate [20]. In 1999, the spinning water atomization process (SWAP) designed and developed by Endo, has been successfully applied to the preparation of $Fe_{73}Si_{10}B_5C_2$ and $(Fe_{0.97}Cr_{0.03})_{76}(Si_{0.5}B_{0.5})_{22}C_2$ amorphous soft magnetic powders [21]. Furthermore, Fe-based amorphous soft

---

*Corresponding author. Tel.: +86-2583587270.

E-mail address: *zhenhuadan@njtech.edu.cn* (Z. Dan)

magnetic powders ($Fe_x(Si_yB_{1-y})_{98-x}C_2$ (x = 73 – 85 at.%, y = 0.2 – 0.9 at.%)) with B_s of 1.64 T have been produced by improved SWAP in 2009, and the Fe contents are further increased [15, 16]. The cooling rates can be achieved as high as 10^{4-5} K/s in the SWAPs. The SWAP with higher cooling rates can be employed to fabricate the powders with ultralow core loss at the high frequency ranges and the high saturated magnetic flux density [21]. The SWAP combines high-speed rotating water to peel off the outer water vapor film on high-temperature droplets to improve the thermal conductivity, high cooling rates as high as about 10^{4-5} K/s in the high-speed rotating water layer and the good powder formation in gas atomization. The above researches give us a hint that the SWAP process has great potential to realize the efficient preparation of NANOMET® powders, break through the size limit of the application of NANOMET® soft magnetic alloys, and obtain superior soft magnetic properties.

The $Fe_{81.3}Si_4B_{10}P_4Cu_{0.7}$ soft magnetic alloy powders were prepared by the spinning water atomization process. The amorphous forming ability, morphology, internal crystalline states, and saturated magnetic flux density of the as-SWAPed powders are to be characterized and analyzed from the sieved powders with different powders sizes. The comparison between as-SWAPed powders and as-spun ribbons has been conducted to clarify the difference in the surface oxide layers and soft magnetic performances.

2. EXPERIMENTAL PROCEDURE

The ingots of $Fe_{81.3}Si_4B_{10}P_4Cu_{0.7}$ alloy were prepared by vacuum induction melting furnace of Fe (99.98 mass %), Si (99.99 mass %), B (99.5 mass %), Cu (99.99 mass %), and pre-alloyed Fe_3P (99.5 mass %), and then cast in a copper mold to form a rod-shaped ingot with a diameter of 10 mm. The $Fe_{81.3}Si_4B_{10}P_4Cu_{0.7}$ alloy powders were fabricated after remelting of as-cast $Fe_{81.3}Si_4B_{10}P_4Cu_{0.7}$ rods by using the spinning water atomization equipment (Fig. 1) under the water pressure at 17.5 MPa, jet gas pressure at 2 MPa, and the setting temperature at 1350 °C. The as-SWAPed powders were sieved into 6 categories according to the range of the powder sizes, i.e.< 20 μm, 20 – 32 μm, 32 – 53 μm, 53 – 75 μm, 75 – 106 μm, and 106 – 150 μm. The counterpart ribbons with a thickness of 18 μm were prepared by melt spinning with the linear velocity of 42 m/s by using rapid solidification of the single copper roller. A differential scanning calorimetry (DSC, Perkin Elmer Co. DSC8500) was used to measure the heat flow behavior and crystallization temperature of the powders during the crystallization process at a heating rate of 40 K/min. The thermal stabilities of as-prepared powders were evaluated by the difference in the primary and secondary crystallization temperatures. The saturated magnetic densities of the sieved powders were measured by Vibrating Sample Magnetometer (Toei Kogyo Co., Ltd. VSM-5) with 7 groups of parallel samples. The sphericity of the powders was observed by scanning electron microscope (SEM, JEOL, FIB4610) under a voltage of 15 kV. The characteristic values of the powder sizes were determined by the laser particle size analyzer. The crystalline state of the as-SWAPed powders was

determined by X-ray diffraction (Rigaku, SmartLab). The as-SWAPed samples were prepared into thin slices using a focused ion beam method (SEM, JEOL FIB4610). The crystalline states and microstructure of powders at the surface, the position at the 1/4 diameter and the middle sites of the individual powders with a diameter of 63 and 26 μm were observed by a transmission electron microscope (TEM, JEOL HC2100). The surface oxide layers on the as-SWAPed powders were analyzed by the Auger electron spectroscope (AES, PHI 710, ULVCA PHI INC.).
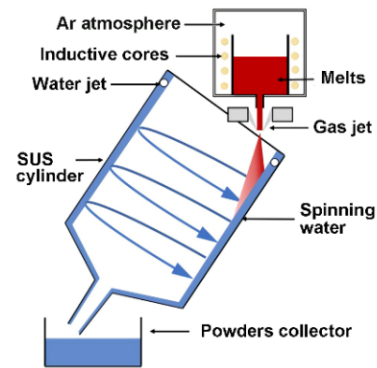

Fig. 1. Schematic setup of the spinning water atomization (SWAP) equipment

3. RESULTS AND DISCUSSION

3.1. Amorphous forming ability and thermal stability of as-SWAPed $Fe_{81.3}Si_4B_{10}P_4Cu_{0.7}$ powders

The morphology of $Fe_{81.3}Si_4B_{10}P_4Cu_{0.7}$ powders prepared by SWAP method with particle size below 150 μm and below 32 μm is shown in Fig. 2.

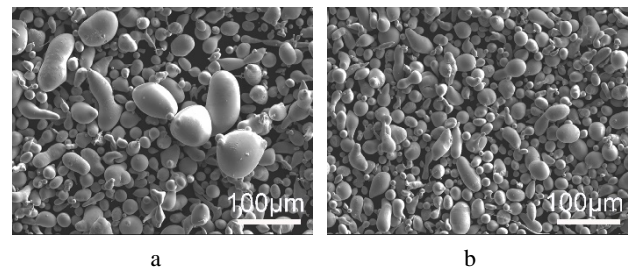**Fig. 2.** SEM morphology of as-SWAPed $Fe_{81.3}Si_4B_{10}P_4Cu_{0.7}$ powders with powder sizes: a – < 150 μm; b – < 32 μm

It is worth stating that the mass of the collected powders occupied 97 % of the total mass of the rods for SWAP. Powders with a particle size larger than 150 μm were accounted for only about 3 %. The accumulated sizes of 50 % powders, d_{50}, of sieved powders with a powder particle size of under 150 μm were 57.8 μm. Fig. 2 a shows that a small amount of ellipsoidal shaped powders with a particle size of over 100 μm existed in sieved powders with a particle size of under 150 μm. As shown in Fig. 2 b, sieved powders with a particle size below 32 μm had good sphericity. Most of the small-sized powders were spherical, and few ellipsoidal or satellite powders coexisted. The powders with a particle size of under 150 μm were sieved into 6 groups according to the particle sizes. As shown in

Fig. 3, the d_{50} values of the powders were confirmed to be 16.5 μm for the powders under 20 μm, 29.6 μm for the powders of 20 – 32 μm, 48.9 μm for the powders of 32 – 53 μm, 71.3 μm for the powders of 53 – 75 μm, 97.8 μm for the powders of 75 – 106 μm, and 143.4 μm for the powders of 106 – 150 μm. The specific values are shown in Table 1.
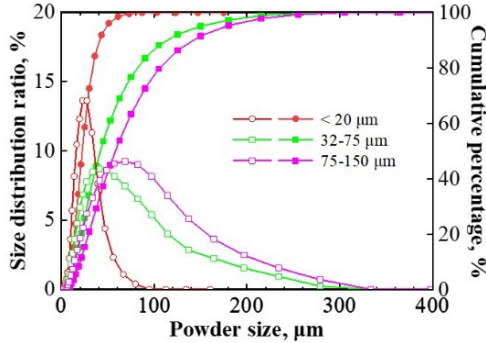

Fig. 3. Size distributions and cumulative percentages of SWAP-ed $Fe_{81.3}Si_4B_{10}P_4Cu_{0.7}$ powders in different powder sizes

It is found that the sphericity of the powders prepared by the SWAP method was worse than gas-atomized powders [10, 12, 17, 18]. This difference is mainly due to the different surface tension and water jet interaction modes during the solidification of the smelt droplets in different preparation processes [17, 18]. It can be seen from Fig. 4 that a broadened diffraction peak at 44.5° in the XRD patterns of as-spun ribbons indicates that the amorphous nature of the as-spun ribbons. The as-SWAPed powders with a particle size of below 150 μm had weak crystal diffraction peaks at 2θ of 44.8° and 82.3° from α-Fe phases.

By comparison, it is found that when the powder size was below 53 μm, there was no diffraction peak from α-Fe. The low diffraction peaks from the as-SWAPed powders with a particle size of 53 – 106 μm are considered to be from the partially crystallized powders consisting of the α-Fe phase. Strong diffraction peaks from α-Fe(110) (200) (211) appeared at 44.5°, 64.9° and 82.3° on the powders with the particle size of 106 – 150 μm, indicating that the amorphous forming abilities of the $Fe_{81.3}Si_4B_{10}P_4Cu_{0.7}$ powders are limited. Fully amorphous powders are hardly obtained for the larger powders due to the limited cooling rates of SWAPs. Based on XRD data, it shows that the as-SWAPed $Fe_{81.3}Si_4B_{10}P_4Cu_{0.7}$ powders had an amorphous forming ability of 53 μm.
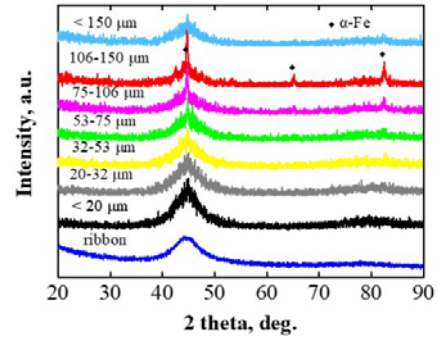

Fig. 4. XRD patterns for as-spun $Fe_{81.3}Si_4B_{10}P_4Cu_{0.7}$ ribbon and as-SWAPed powders with powder sizes

The thermal stabilities of as-SWAPed powders are evaluated by the DSC analysis. As shown in Fig. 5, the DSC curves of $Fe_{81.3}Si_4B_{10}P_4Cu_{0.7}$ powders were similar with that of the counterpart ribbons, which all contain the primary crystallization exothermic peaks of the α-Fe phases and the secondary crystallization exothermic peaks of the Fe-B phases.

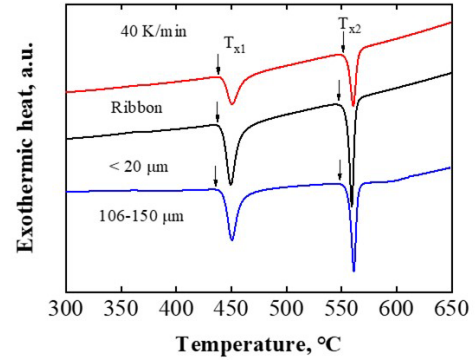**Fig. 5.** DSC curves of as-spun $Fe_{81.3}Si_4B_{10}P_4Cu_{0.7}$ ribbon and as-SWAPed powders with powder sizes. Heating rate is set at 40 K/min

The initial crystallization temperature (T_{x1}) of $Fe_{81.3}Si_4B_{10}P_4Cu_{0.7}$ amorphous ribbons was confirmed to be 441.9 °C, and the second crystallization temperature (T_{x2}) was 557.0 °C. On basis of the collected data of the crystallization temperature T_{x2} and T_{x1} of $Fe_{81.3}Si_4B_{10}P_4Cu_{0.7}$ powders with different particle sizes summarized in Table 1.

Table 1. Summary of d_{50}, crystallization temperature T_{x1} and T_{x2}, exothermic heat ΔH_1 and ΔH_2, coercivity H_c, saturated magnetic flux density M_s and the crystalline state of as-quenched $Fe_{81.3}Si_4B_{10}P_4Cu_{0.7}$ ribbons and SWAP-ed powders with different powder sizes

Powder group, μm	d_{50}, μm	T_{x1}, °C	ΔH_1, J/g	T_{x2}, °C	ΔH_2, J/g	ΔT, °C	$H_c{}^*$, A/m	B_m, emu/g	Crystalline state
Ribbon	-	441.9	58.3	557.0	49.7	115.1	34.2	174.4	F
< 20	16.5	439.5	56.6	554.9	47.6	115.4	37.1	173.7	F
20 – 32	29.6	440.7	57.8	553.5	46.6	112.8	37.5	169.4	F
32 – 53	48.9	440.3	57.0	553.6	47.6	113.3	37.1	173.6	F
53 – 75	71.3	440.8	55.2	554.2	45.6	113.4	38.5	173.0	F
75 – 106	97.8	441.4	50.5	555.2	42.2	113.8	39.4	173.0	P
106 – 150	143.4	442.0	32.6	554.7	29.2	112.7	41.8	177.7	P
$H_c{}^*$: obtained from VSM measurements; F: fully amorphous; P: partially crystalline									

It can be seen that there was no significant difference in T_{X2} and T_{X1} between the powders with different particle sizes except for the powders with large particle sizes in the range of $75-106$ μm and $106-150$ μm which was slightly lower than the crystallization temperature of the as-spun ribbons. The temperature difference between T_{X2} and T_{X1}, ΔT, can be regarded as a criterion to reflect the thermal stability of the amorphous materials. A wider temperature window (larger ΔT) for the crystallization reactions is expected for the Fe-based amorphoheterogeneous soft magnetic alloys. As shown in Table 1, the ΔT values of the powders and the ribbons were similar. The ΔT of amorphous powders was between 112.8 and 115.4 K, while the ΔT of partially crystalline powders was between 112.7 and 113.8 K. By comparing the enthalpy change (ΔH_1) of the crystallization process of the α-Fe phases and the enthalpy change (ΔH_2) of the crystallization process of the Fe-B second phases in the counterpart ribbons and powders with different particle sizes, it can be found that the enthalpy change, ΔH_1 and ΔH_2, gradually become smaller as the particle size increases, indicating that there is a higher proportion of crystallized α-Fe and Fe-B phases distributed in the larger-sized powders. For example, the content of α-Fe phases in powders with a particle size of $106-150$ μm had reached more than 42 %. The experimental data of XRD patterns (Fig. 4) and DSC curves (Fig. 5) show that the partial crystallization and the precipitation of α-Fe phases occurred in the large-sized as-SWAPed powders due to the limited amorphous forming ability of Fe-based amorphous alloys and the relative lower cooling rates of SWAP than melt spinning. As the particle size of the powders increased, the volume fractions of the α-Fe phases increased, and the thermal stability of the amorphous matrix became worse. On the other hand, there might be some differences in the microstructures and the thickness of the surface oxide films of the powders and the ribbons due to the difference in the cooling rates and the reaction of the powder surface after contacting with cooling water in the SWAP process and the rapid solidification process.

3.2. Crystalline states and soft magnetic properties of as-SWAPed $Fe_{81.3}Si_4B_{10}P_4Cu_{0.7}$ powders

The single powder with a particle size of 63 μm was selected to be processed into a TEM sample by the focused ion beam method. The microstructure and crystalline states of different parts of the powder were observed. As shown in Fig. 6 a, FIB-SEM morphology of several powders with good sphericity show that processing defects (i.e. unevenly distributed grooves) were caused during the FIB slicing process. Based on the bright field image analysis at the sites of the outmost layers of the powder (Fig. 6 b 1), the position at the 1/4 diameters of the powder (Fig. 6 b 2) and the center of the powder (Fig. 6 b 3), it is found that the internal structure was uniform and no large size crystalline precipitates were found, and the electron diffraction pattern selected (Fig. 6 c 1–3) were all typical amorphous diffraction patterns.

This could be caused by the heat transfer and heat accumulation inside the center [5, 9, 17, 18]. The FIB-SEM images (Fig. 7 a) and the bright field TEM images of the microstructure, selected area electron diffraction, and high-

resolution TEM images (Fig. 7 b, d) observation results of the $Fe_{81.3}Si_4B_{10}P_4Cu_{0.7}$ powders with a smaller particle size of 22 μm show that the small particle size powders had uniform amorphous structure and no fine precipitated crystalline clusters.
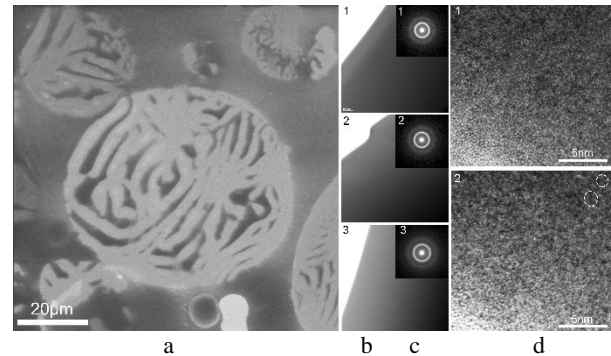

Fig. 6. a – FIB-SEM image; b – bright field TEM images; c – selected area diffraction patterns of SWAP-ed $Fe_{81.3}Si_4B_{10}P_4Cu_{0.7}$ powders with different powder size of $53-75$ μm at the edge (b1, c1), 1/4D (b2, c2) and central (b3, c3) region. High-resolution TEM images are taken at the central (d1) and edge (d2) regions of the powders
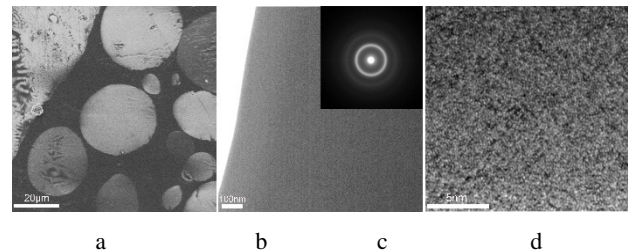

Fig. 7. a – FIB-SEM image; b – bright field TEM images; c – selected area diffraction patterns; d – high-resolution TEM images of as-SWAPed $Fe_{81.3}Si_4B_{10}P_4Cu_{0.7}$ powders with powder size of $20-32$ μm

The soft magnetic properties of $Fe_{81.3}Si_4B_{10}P_4Cu_{0.7}$ powders prepared by the SWAP method were evaluated by the hysteresis loop of VSM. As shown in Fig. 8 a, ribbons with a thickness of 18 μm can quickly reach a magnetically saturated state ($B_m = 174.4$ emu/g) under the action of a 5 KOe external magnetic field, and completely amorphous powders with a particle size of less than 20 μm had B_m of 173.7 emu/g. Partially crystallized powders with a particle size of $106-150$ μm exhibit B_m of 177.7 emu/g, which is slightly higher than that of amorphous ribbons and amorphous powders. The coercivity, H_c, of the ribbons and powders with different particle sizes was confirmed to be 34.2~41.8 A/m by VSM as listed in Table 1. The above-mentioned phenomenon shows that the $Fe_{81.3}Si_4B_{10}P_4Cu_{0.7}$ powders prepared by the SWAP method can reach the saturation state only under the condition of a large external magnetic field. The relationship between B_m and the change of powder particle size is shown in Fig. 8 b. A slight change of B_m locates between 169.4 and 173.7 emu/g. Based on the data of XRD (Fig. 3), DSC (Fig. 4), and TEM (Fig. 7 and Fig. 8), it can be seen that the amorphous powders with a particle size below 53 μm have higher B_m.

In the HRTEM image of the $Fe_{81.3}Si_4B_{10}P_4Cu_{0.7}$ powders with a particle size of $53-75$ μm (Fig. 9 a), it can be seen that the surface of the as-SWAPed powders had a

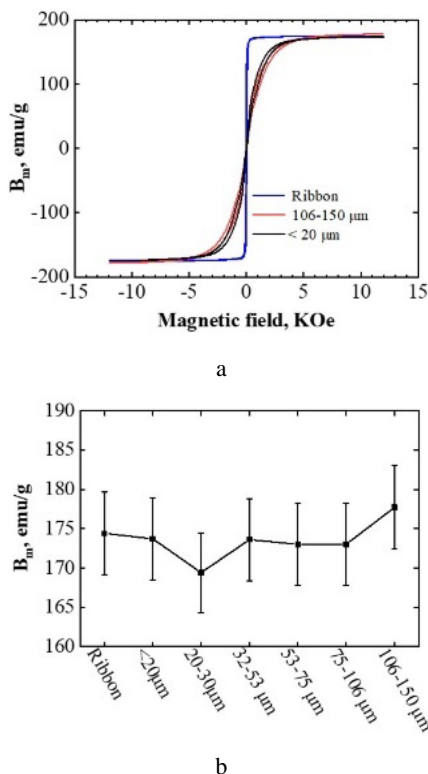smooth appearance and a uniform oxide layer with a thickness of about 10 nm.

a

b

Fig. 8. a – B-H loops of as-spun $Fe_{81.3}Si_4B_{10}P_4Cu_{0.7}$ ribbon and as-SWAPed powders with powder size of under 20 μm and 106 – 150 μm, b – the change of the saturated magnetic flux density versus different powder sizes
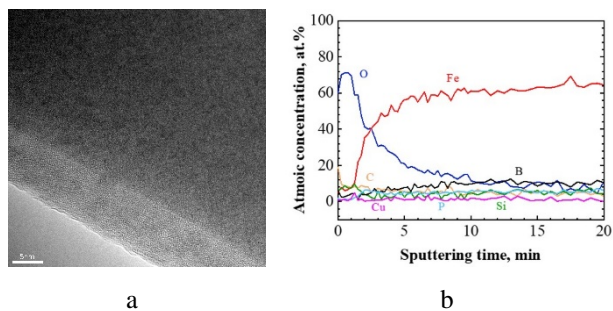

a   b

Fig. 9. a – the high-resolution TEM images; b – AES spectra of as-SWAPed $Fe_{81.3}Si_4B_{10}P_4Cu_{0.7}$ powders with a powder size of 53 – 75 μm

No crystalline phase was detected in the oxide layer, indicating that the oxide layer is composed of amorphous oxide. The results of the AES analysis (Fig. 9 b) show that Cu and Si are enriched at the interface. It also can be inferred that the main component of the outmost oxide is adsorbed CO_2, while the inner oxide is mainly composed of Fe_3O_4 and SiO_2 according to the ratio of the chemical elements. The thickness of the surface oxide layer on the ribbons prepared by the rapid solidification method in an open-air environment has been reported to be about 3 – 5 nm [23]. However, the surface oxidation took place after the smelt droplets reacted with water in the SWAP process. Under the effects of both the large reaction specific surface area of the powders and the high temperature, the surface oxide layer with the thickness of 10 nm was formed, which is mainly composed of Fe_3O_4 and SiO_2.

3.3. Discussion

The above-presented data show that the amorphous forming ability of $Fe_{81.3}Si_4B_{10}P_4Cu_{0.7}$ powders prepared by SWAP method is 53 μm, indicating that the SWAP method is beneficial to improve the amorphous forming ability of powders. The critical thickness of amorphous $Fe_{78}Si_9B_{13}$ bulks prepared by the two-step method can reach 150 μm after stacking the slices with a thickness of 3 μm [24]. Although it shows the better amorphous forming ability, it is limited to two-dimensional stacking mode [24]. On the other hand, composition design can also effectively improve the amorphous forming ability. For example, in the $Fe_{81.2}Si_{0.5}B_{9.5}P_4Cu_{0.8}$ system, the amorphous forming ability of $Fe_{85.2}Co_4Si_{0.5}B_{9.5}P_4Cu_{0.8}$ and $(Fe_{85.2}Co_4Si_{0.5}B_{9.5}P_4Cu_{0.8})_{99}C_1$ can be increased from 20 μm to 43 μm by adding Co or C, which broadens the applications of high-B_s NANOMET® soft magnetic alloys [5, 6, 25, 26]. For the amorphous powders, optimization of the preparation method can also improve their amorphous forming ability. The amorphous forming ability of the aerosolized $Fe_{76}Si_9B_{10}P_5$ powders with low Fe content was close to 53 μm, while the $Fe_{81.5}Si_{0.5}B_{4.5}P_{11.0}Cu_{0.5}C_{2.0}$ powders prepared under the same processing conditions formed an amorphous state only when its particle size was below 10 μm [27]. Yoshida has prepared $Fe_{81}Si_{11.9}B_{5.7}P_{11.4}$ Fe-based amorphous powders with high Fe content by the combination of gas atomization and composition design, while $Fe_{81}Si_3B_6P_{10}$ and $Fe_{81}Si_{1.5}B_5P_{12.5}$ powders prepared by the same method have generated a large amount of Fe_3B crystals in the preparation process, indicating that their thermal ability to maintain the amorphous state is very limited [17]. Although XRD results show that the powders are amorphous, XRD analysis cannot accurately distinguish the amorphous nanocrystalline alloy with grain size less than 7 nm [28]. However, the TEM analysis results show that there were fine crystalline clusters with the size of about 3 nm in the gas-atomized powders. This type of Heteroamorphous structure is typical for the rapid-solidified ribbons of NANOMET® soft magnetic alloys. Only a few tiny crystallized clusters with the size of 1 – 2 nm can be seen in the as-SWAPed powders (Fig. 6 d 2). The amorphous forming ability of the $Fe_{81.3}Si_4B_{10}P_4Cu_{0.7}$ powders prepared by the SWAP method can reach 53 μm, indicating that the SWAP method is beneficial to improve the amorphous forming ability of NANOMET® powders. The B_m of the powders after the fracture of the amorphous $Fe_{78}Si_9B_{13}$ ribbons was 164 emu/g [29]. The spray cooling gas atomization method greatly improved the cooling effect, and the amorphous forming ability of the as-prepared $Fe_{76}Si_9B_{10}P_5$ powders increases to 63 μm and its B_m can reach 156 emu/g. The composition analysis of Fe-based alloys (i.e. TZ220, TZ560, and TZ611) prepared by the spray cooling gas atomization state that the surface oxide layer becomes thicker after contacting with the spray water [20]. The formation of the surface oxides on the powders is helpful to reduce the electrical conductivity between the powder particles, which is beneficial to reduce the core loss caused by the eddy current effect. 3 nm SiO_2 coating layer on the gas atomized $Fe_{76}Si_9B_{10}P_5$ powders can keep the powders in an insulating state at a high frequency of 3 GHz [30].

319

However, the B_m had only a small decrease (from 164 emu/g to 161 emu/g), and higher external magnetic fields are required to reach the magnetic saturation state. The same tendency of surface oxidation to decrease the saturated magnetic density has been found on amorphous $Fe_{78}Si_9B_{13}$ oxidized at high temperatures [31]. The findings above presented can be regarded as the reasons why the saturated magnetic density of as-SWAPed $Fe_{81.3}Si_4B_{10}P_4Cu_{0.7}$ powders was slightly decreased and the external magnetic field intensity increased to reach the saturation state (Fig. 8). Compared with $Fe_{76}Si_9B_{10}P_5$ and $Fe_{78}Si_9B_{13}$ powders, B_m of as-SWAPed $Fe_{81.3}Si_4B_{10}P_4Cu_{0.7}$ powders can reach 173 emu/g, which was increased more than 10 %, and higher saturated magnetic density was obtained. Meanwhile, an insulating oxide film with eddy current resistance was formed on the surface of the powders. The $Fe_{81.3}Si_4B_{10}P_4Cu_{0.7}$ amorphous powders fabricated by SWAP with ultralow core loss and high saturated magnetic flux density are expected to better application in high-performance miniaturized electronic products.

4. CONCLUSIONS

The nearly spherical $Fe_{81.3}Si_4B_{10}P_4Cu_{0.7}$ soft magnetic powders with a particle size of $0-150\ \mu m$ up to 97 % were prepared by the spinning-water atomization process (water pressure: 17.5 MPa; air pressure: 2 MPa). The as-prepared powders were divided into 6 groups of different particle size ranges below $20\ \mu m$, $20-32\ \mu m$, $32-53\ \mu m$, $53-75\ \mu m$, $75-106\ \mu m$ and $106-150\ \mu m$ by grading sieve, which were used to confirm the amorphous forming ability, the amount of α-Fe and the change of soft magnetic properties at different particle sizes. The experimental analysis results show that the $Fe_{81.3}Si_4B_{10}P_4Cu_{0.7}$ powders prepared by spinning-water atomization process had good sphericity and amorphous forming ability of 53 μm, and the saturated magnetic density of the completely amorphous powders was $170-173$ emu/g, and the thermal stability of the amorphous matrix can reach more than 112.8 K, which is comparable to the performance of the amorphous ribbon prepared by the rapid solidification method. The oxide film with a thickness of 10 nm, mainly composed of Fe_3O_4 and SiO_2, was formed on the powders. Although the saturated magnetic flux density was slightly reduced, it is beneficial to reduce the eddy current effects.

REFERENCES

1. **Suzuki, K., Makino, A., Kataoka, N., Kataoka, N., Inoue, A., Masumoto, T.** High Saturation Magnetization and Soft Magnetic Properties of bcc Fe-Zr-B and Fe-Zr-B-M (M=Transition Metal) Alloys with Nanoscale Grain Size *Materials Transactions JIM* 32 (1) 1991: pp. 93 – 102.

2. **Yoshizawa, Y., Oguma, S., Yamauchi, K.** New Fe-based Soft Magnetic Alloys Composed of Ultrafine Grain Structure *Journal of Applied Physics* 64 (10) 1988: pp. 6044 – 6046. https://doi.org/10.1063/1.342149

3. **Yoshizawa, Y., Yamauchi, K.** Fe Based Soft Magnetic Alloys Composed of Ultrafine Grain Structure *Japan Institute of Metals and Materials* 53 (2) 1989: pp. 241 – 248. https://doi.org/10.2320/jinstmet1952.53.2_241

4. **Wakiyama, T., Takahashi, M., Nishimaki, S., Shimoda, J.** Magnetic Properties of Fe-Si-Al Single Crystals *IEEE Transactions on Magnetics* 17 (6) 1981: pp. 3147 – 3150. https://doi.org/10.1109/TMAG.1981.1061694

5. **Takenaka, K., Setyawan, A.D., Sharma, P., Nishiyama, N., Makino, A.** Industrialization of Nanocrystalline Fe-Si-B-P-Cu Alloys for High Magnetic Flux Density Cores *Journal of Magnetism and Magnetic Materials* 401 2016: pp. 479 – 483. https://doi.org/10.1016/j.jmmm.2015.10.091

6. **Makino, A.** Nanocrystalline Soft Magnetic Fe-Si-BP-Cu Alloys with High *B* of 1.8-1.9T Contributable to Energy Saving *IEEE Transactions on Magnetics* 48 (4) 2012: pp. 1331 – 1335. https://doi.org/10.1109/TMAG.2011.2175210

7. **Mallick, S., Sharma, P., Takenaka, K., Makino, A., Bedanta, S.** Static and Dynamic Behavior of Domain Walls in High B_s Soft Magnetic Ribbons Tuned by the Annealing Temperature *Journal of Physics D* 51 (6) 2018: pp. 065007. https://doi.org/10.1088/1361-6463/aaa43d

8. **Takeuchi, A., Zhang, Y., Takenaka, K., Makino, A.** Thermodynamic Analysis of Binary $Fe_{85}B_{15}$ to Quinary $Fe_{85}Si_2B_8P_4Cu_1$ Alloys for Primary Crystallizations of α-Fe in Nanocrystalline Soft Magnetic Alloys *Journal of Applied Physics* 117 (17) 2015: pp. 17B737. http://dx.doi.org/10.1063/1.4918689

9. **Makino, A., Men, H., Kubota, T., Yubuta, K., Inoue, A.** New Excellent Soft Magnetic FeSiBPCu Nanocrystallized Alloys with High B_s of 1.9T from Nanohetero-amorphous Phase *IEEE Transactions on Magnetics* 45 (10) 2009: pp. 4302 – 4305. https://doi.org/10.1109/TMAG.2009.2023862

10. **Nishiyama, N., Takenaka, K., Miura, H., Saidoh, N., Zeng, Y.Q., Inoue, A.** The World's Biggest Glassy Alloy everMade*Intermetallics* 30 2012: pp. 19 – 24. https://doi.org/10.1016/j.intermet.2012.03.020

11. **Paul, T., Chawake, N., Kottada, R.S., Harimkar, S.P.** Pressure Controlled Micro-viscousDeformation Assisted Spark Plasma Sintering of Fe-based Bulk Amorphous Alloy*Journal of Alloys and Compounds* 738 2018: pp. 10 – 15. https://doi.org/10.1016/j.jallcom.2017.12.147

12. **Mahbooba, Z., Thorsson, L., Unosson, M., Skoglund, P., West, H., Horn, T., Rock, C., Vogli, E., Harrysson, O.** Additive Manufacturing of an Iron-based Bulk Metallic Glass Larger than the Critical Casting Thickness *Materials Today Applied Materials* 11 2018: pp. 264 – 269. https://doi.org/10.1016/j.apmt.2018.02.011

13. **Jung, H.Y., Choi, S.J., Prashanth, K.G., Stoica, M., Scudino, S., Yi, S., Kühn, U., Kim, D.H., Kim, K.B., Eckert, J.** Fabrication of Fe-based Bulk Metallic Glass by Selective Laser Melting: a Parameter Study *Materials and Design* 86 2015: pp. 703 – 708.
https://doi.org/10.1016/j.matdes.2015.07.145

14. **Li, N., Zhang, J., Xing, W., Ouyang, D., Liu, L.** 3D Printing of Fe-based Bulk Metallic Glass Composites with Combined High Strength and Fracture Toughness *Materials and Design* 143 2018: pp. 285 – 296.
https://doi.org/10.1016/j.matdes.2018.01.061

15. **Otsuka, I., Wada, K., Maeta, Y., Kadomura, T., Yagi, M.** Magnetic Properties of Fe-Based Amorphous Powders with High-Saturation Induction Produced by Spinning Water Atomization Process (SWAP) *IEEE Transactions on Magnetics* 44 (11) 2018: pp. 3891 – 3894.
https://doi.org/10.1109/TMAG.2008.2002249

16. **Otsuka, I., Maeta, Y., Ishiyama, K., Yagi, M.** The Characteristic of High Magnetic Flux Density Fe-based Amorphous Soft Magnetic Powders and Consolidated Magnetic Cores *Journal of Japan Powder and Powder Metallurgy* 56 (9) 2009: pp. 563 – 567.
https://doi.org/10.2497/jjspm.56.563

17. **Yoshida, K., Bito, M., Kageyama, J., Shimizu, Y., Abe, M., Makino, A.** Unusual High B_s for Fe-based Amorphous Powders Produced by a Gas-atomization Technique *AIP Advances* 6 (5) 2016: pp. 055933.
https://doi.org/10.1063/1.4944765

18. **Takahashi, T., Yoshida, K., Shimizu, Y., Setyawan, A.D., Bito, M., Abe, M., Makino, A.** Fe-Si-B-P-C-Cu Nanocrystalline Soft Magnetic Powders with High B_s and Low Core Loss *AIP Advances* 7 (5) 2017: pp. 056111.
https://doi.org/10.1063/1.4978408

19. **Oleszak, D., Matyja, H.** Nanocrystalline Fe-based Alloys Obtained by Mechanical Alloying *Nanostructured Materials* 6 (1 – 4) 1995: pp. 425 – 428.
https://doi.org/10.1016/0965-9773(95)00087-9

20. **Liu, K.J., Le, C., Zhao, F. Tang, M.Q., Wu, C.Y.** The Microstructure and Soft Magnetic Properties of $Fe_{72}Si_{10.7}B_{10.7}Cr_{2.2}P_{1.5}C_{2.9}$ Magnetic Powders Produced by Water-gas Atomization *Journal of Magnetic Materials and Devices* 49 (6) 2018: pp. 10 – 13.
https://doi.org/10.19594/j.cnki.09.19701.2018.06.003

21. **Endo, I., Otsuka, I., Okuno, R., Shintani, A., Yoshino, M., Yagi, M.** Fe-based Amorphous Soft-magnetic Powder Produced by Spinning Water Atomization Process (SWAP) *IEEE Transactions on Magnetics* 35 (5) 1999: pp. 3385 – 3387.
https://doi.org/10.1109/20.800532

22. **Dan, Z.H., Zhang, Y., Takeuchi, A., Hara, N., Qin, F.X., Makino, A., Chang, H.** Effect of Substitution of Cu by Au and Ag on NanocrystallizationBehavior of $Fe_{83.3}Si_4B_8P_4Cu_{0.7}$ Soft Magnetic Alloy *Journal of Alloys and Compounds* 683 2016: pp. 263 – 270.
https://doi.org/10.1016/j.jallcom.2016.05.027

23. **Dan, Z.H., Takenaka, K., Zhang, Y., Unami, S., Takeuchi, A., Hara, N., Makino, A.** Effect of Si Addition on the Corrosion Properties of Amorphous Fe-based Soft Magnetic Alloys *Journal of Non-Crystalline Solids* 402 2014: pp. 36 – 43.
https://doi.org/10.1016/j.jnoncrysol.2014.05.007

24. **Oguchi, M., Harakawa, Y., Inoue, A., Masumoto, T.** Production of Flaky Fe-based Amorphous Powders by a Two-stage Quenching Technique and Their Magnetic Properties *Materials Science and Engineering: A* 181 1994: pp. 1161 – 1164.
https://doi.org/10.1016/0921-5093(94)90823-0

25. **Geng, Y.X., Wang, Y.M.** Local Structure-property Correlation of Fe-based Amorphous Alloys: Based on Minor Alloying Research *Acta Metallurgy Sinca* 56 (11) 2020: pp. 1558 – 1568.
https://doi.org/10.11900/0412.1961.2020.00112

26. **Xu, M., Sun, Y., Quan, M.X., Wang, Y.D., Zuo, L.** Glass-forming Ability and Soft Magnetic Properties of Fe-Co-Nd-Nb-B Amorphous Alloys *Acta Metallurgy Sinca* 43 (7) 2007: pp. 699 – 704.

27. **Suzuki, T., Sharma, P., Jiang, L.X., Zhang, Y., Makino, A.** Fabrication and Properties of under 10μm Sized Amorphous Powders of High B_s Soft Magnetic Alloy for High-frequency Applications *IEEE Transactions on Magnetics* 54 (11) 2018: pp. 1 – 5.
https://doi.org/10.1109/TMAG.2018.2833138

28. **Jiang, J.Z., Saida, J., Kato, H., Ohsuna, T., Inoue, A.** Is $Cu_{60}Ti_{10}Zr_{30}$ a Bulk Glass-forming Alloy? *Applied Physics Letters* 82 (23) 2003: pp. 4041 – 4043.
https://doi.org/10.1063/1.1581001

29. **Li, Z.C., Dong, Y.Q., Li, F.S., Chang, C.T., Wang, X.M., Li, R.W.** $Fe_{78}Si_9B_{13}$ Amorphous Powder Core with Improved Magnetic Properties *Journal of Materials Science* 28 (2) 2017: pp. 1180 – 1185.
https://doi.org/10.1007/s10854-016-5644-5

30. **Suzuki, T., Sharma, P., Makino, A.** Extending the Operational Frequency range of High B_s-FeSiBP Amorphous Alloy to GHz by Coating the Powder Surface with Silicon Oxide *Journal of Magnetism and Magnetic Materials* 491 2019: pp. 165641.
https://doi.org/10.1016/j.jmmm.2019.165641

31. **Zhu, Z.H., Yin, L., Hu, Q., Song, H.** Influence of High-Temperature Oxidation on Soft Magnetic Properties of $Fe_{78}Si_9B_{13}$ Amorphous Alloy *Rare Metal Materials and Engineering* 43 (5) 2014: pp. 1037 – 1040.
https://doi.org/10.1016/S1875-5372(14)60096-5